

Time-dependent blood flow and oxygenation in human skeletal muscles measured with noninvasive near-infrared diffuse optical spectroscopies

Guoqiang Yu
Turgut Durduran

University of Pennsylvania
Department of Physics and Astronomy
Philadelphia, Pennsylvania 19104

Gwen Lech

University of Pennsylvania
Department of Biochemistry and Biophysics
Philadelphia, Pennsylvania 19104

Chao Zhou

University of Pennsylvania
Department of Physics and Astronomy
Philadelphia, Pennsylvania 19104

Britton Chance

University of Pennsylvania
Department of Biochemistry and Biophysics
Philadelphia, Pennsylvania 19104

Emile R. Mohler III

University of Pennsylvania
School of Medicine
Department of Medicine, Cardiovascular Division
Philadelphia, Pennsylvania 19104

Arjun G. Yodh

University of Pennsylvania
Department of Physics and Astronomy
Philadelphia, Pennsylvania 19104

Abstract. We have employed near-infrared optical methods to measure noninvasively the dynamics of muscle blood flow and oxygen saturation (S_tO_2) during cuff occlusion and plantar flexion exercise. Relative muscle oxygen consumption (rVO_2) was also computed from these data. Diffuse correlation spectroscopy provides information about blood flow, and diffuse reflectance spectroscopy provides information about blood oxygenation. Ten healthy subjects and one patient with peripheral arterial disease (PAD) were studied during 3-min arterial cuff occlusion of arm and leg, and during 1-min plantar flexion exercise. Signals from different layers (cutaneous tissues and muscles) during cuff occlusion were differentiated, revealing strong hemodynamic responses from muscle layers. During exercise in healthy legs, the observed ~ 4.7 fold increase in relative blood flow (rBF) was significantly lower than the corresponding increase in rVO_2 (~ 7 fold). The magnitudes of rBF and rVO_2 during exercise in the PAD patient were $\sim 1/2$ of the healthy controls, and the S_tO_2 recovery time was twice that of the controls. The hybrid instrument improves upon current technologies for measuring muscle responses by simultaneously measuring rBF and S_tO_2 . The instrument thus provides a method for evaluation of microcirculation and muscle metabolism in patients with vascular diseases. © 2005 Society of Photo-Optical Instrumentation Engineers. [DOI: 10.1117/1.1884603]

Keywords: dynamic light scattering; photon migration; light diffusion; diffuse correlation spectroscopy; diffuse reflectance spectroscopy; near-infrared spectroscopy; arterial cuff occlusion; plantar flexion exercise; peripheral arterial disease.

Paper JBO 04098R received Jun. 11, 2004; revised manuscript received Sep. 30, 2004; accepted for publication Nov. 2, 2004; published online Apr. 11, 2005.

1 Introduction

Noninvasive characterization of oxygen consumption and metabolism in skeletal muscles has important applications in exercise medicine^{1,2} and for understanding of vascular conditions such as peripheral arterial disease (PAD).^{3,4} Improved measurements of these quantities may lead to improved screening and treatment assessment, as well as to improved fundamental understanding of muscle function.

Over the years, a variety of noninvasive techniques have been developed to study tissue hemodynamics of muscle. Conventional venous occlusion plethysmography has been employed for more than 50 years in muscle perfusion investigations.^{5,6} This method, however, does not provide regional information and can be used only in the static state or during brief exercise, since venous occlusion interrupts blood flow. Ultrasound Doppler is a common clinical tool used to measure blood flow in large vessels.^{7,8} However it is not sensitive to flow in smaller vessels, and does not readily permit continuous measurements during exercise. Laser Doppler can

noninvasively monitor flow changes, but most systems measure the tissue surface only (i.e., penetration depth $< 500 \mu\text{m}$);^{9,10} very recently, Binzoni et al. have extended its application to relatively deeper tissues using larger source-detector separations (1.5 cm).¹¹ Magnetic resonance spectroscopy or imaging (MRS/MRI) has high temporal and spatial resolution,¹² however, its clinical use is limited due to high cost and poor mobility. Positron emission tomography (PET) has similar clinical limitations, and also has poor spatiotemporal resolution compared to MRS/MRI.¹³

Near-infrared spectroscopy (NIRS) has the potential to fill part of this void. Unlike ultrasound Doppler, it is sensitive to smaller vessels such as arterioles, capillaries, and venules.¹⁴ In principle it can provide dynamic information about oxygen and deoxy-hemoglobin concentrations, total hemoglobin concentration (THC), and tissue blood oxygen saturation (S_tO_2) in deep muscle tissues.^{3,15} It provides high temporal resolution, relatively low spatial resolution, and is inexpensive and portable. Previously blood flow and oxygen consumption in muscle tissue have been estimated from changes of THC or

Address all correspondence to Guoqiang Yu, University of Pennsylvania, Dept. of Physics and Astronomy, Philadelphia, PA 19104. Tel: (215)573-3463; Fax: (215)573-6391; E-mail: guoqiang@physics.upenn.edu

deoxy-hemoglobin concentration by applying venous or arterial occlusion to a limb;^{16–18} unfortunately, these applications of NIRS to flow studies face the same limitations as venous occlusion plethysmography.

Near-infrared diffuse correlation spectroscopy (DCS) is an emerging technique for continuous noninvasive measurement of relative blood flow in deep tissues. It has been successfully applied in studies of brain hemodynamics,^{19,20} photodynamic therapy (PDT) dosimetry,²¹ and for measurement of tissue burn depth.²² Measurements of relative blood flow by DCS have also been validated against color power Doppler ultrasound in animal tumor studies^{21,23} and laser Doppler in animal brain studies.^{19,20} DCS enables measurements of relative blood flow (rBF) with high temporal (~ 100 ms) and limited spatial (\sim mm) resolution in tissue. To date most applications of DCS have been in small animal studies wherein source-detector separations were comparatively small (< 1 cm).^{19–23} Very recently, DCS measurements have been performed through an adult human skull with source-detector separations up to 3 cm.²⁴ Nevertheless, the major challenge for human applications remains; improvement of DCS signal-to-noise at the large source-detector separations is necessary to probe through thick near-surface tissue layers above muscle, e.g., skin and adipose tissue.

The lack of portable, noninvasive technologies for continuous monitoring of both blood flow and oxygenation in the deep microcirculation (capillary bed) has led us to develop a hybrid instrument combining near-infrared DCS and diffuse reflectance spectroscopy (DRS).^{19,20} DCS monitors blood flow by effectively measuring the optical phase shifts caused by moving blood cells, while DRS measures tissue optical properties (absorption and scattering). The purpose of this paper is to report concurrent measurements of blood flow and oxygenation in cuffed and exercising human muscle. To our knowledge we demonstrate the first clinical use of DCS for monitoring flow dynamics in muscle, and the first clinical use of all-optical methods for simultaneously measuring multiple hemodynamic parameters in muscle. These hemodynamic parameters include relative blood flow (rBF), tissue blood oxygen saturation (S_tO_2), and total hemoglobin concentration (THC), permitting estimation of changes in oxygen metabolism.

2 Materials and Methods

2.1 Protocols

The experimental protocol used in this study has three parts: cuff occlusion of the arm flexor, cuff occlusion of the thigh, and plantar flexion (PF) exercise. For cuff occlusion of arm and leg, the subjects were asked to lie supine. The optical probe was placed over the wrist flexor or calf flexor (medial gastrocnemius) and secured with an elastic bandage. After 3 min of resting baseline measurements, the blood pressure cuff was manually inflated to 180 mmHg for arm and 220 mmHg for leg, held for 3 min, and then rapidly released. The recovery measurement was made for approximately 3 min. For the plantar flexion exercise, the subjects remained in a stable standing position during the test protocol. Both legs were positioned at shoulder width and the probe was placed over the calf flexor. After a 3-min baseline, the subjects performed 30 plantar flexion exercises (toe up-downs) within one minute,

followed by a 3-min recovery measurement. In addition, a skinfold caliper (Beta Technology Inc., Cambridge, Maryland) was used to mechanically measure the thickness of the upper layers (skin and adipose) above muscle.

Cuff occlusion was used to investigate the different layer responses in order to estimate light penetration depth and to validate results in the ischemic states. The hemodynamic response to extended cuff occlusion has been thoroughly measured and characterized and is a good model for validation of our results. Plantar flexion exercise was selected because it selectively works the gastrocnemius muscle and can be performed by patients with peripheral arterial disease (PAD). This muscle is used in both stair climbing and walking. We chose to study a PAD patient because insufficient blood supply to this muscle in PAD patients commonly results in symptomatic calf pain and walking disability. PAD affects an estimated 25% of the elderly population in North America.²⁵ Thus improvements in technology to screen and assess PAD treatment can have a substantial impact. All healthy volunteers rated the intensity of the 30-min plantar flexion exercise as an easy-to-somewhat-difficult exercise. No healthy volunteer experienced leg discomfort. The PAD subject experienced slight cramping pain after ~ 20 plantar flexion exercises.

The studies were approved by the Institutional Review Board (IRB) at the University of Pennsylvania and took place at the Hospital of the University of Pennsylvania. Ten healthy subjects (eight males and two females) with ages between 24–34 years (28.4 ± 3.0), and one male PAD patient, age 65, were measured. The ankle brachial index (ABI) of the healthy subjects was 1.01 ± 0.02 . The ABI of the PAD patient was 0.4 in the leg studied; this index is considered severe PAD according to the Rutherford-Becker Classification.²⁶

2.2 Instrumentation

The instrument is described in detail elsewhere.^{19,20} Figure 1(b) shows a schematic of the hybrid instrument. Briefly, lasers at three wavelengths (676 nm, 786 nm, 830 nm) modulated at 70 MHz (frequency domain) were used for DRS measurements; a continuous-wave laser (800 nm) with a long coherence length was used for DCS. Two sets of avalanche photodiodes (APD) were employed for DRS and DCS measurements. The probe, shown in Fig. 1(a), had eight DCS detector fibers (empty squares) at the periphery of concentric circles around one DCS source fiber (cross, S1), and four DRS detector fibers (solid circles, D1 to D4) with six DRS source fibers (empty circles, S1 to S6) arranged on a 3-cm radius circle. Note that the DRS source position S1 (open circle) overlaps with the DCS source position S1 (cross); the same source fiber was shared by both lasers. Source-detector separations ranged from 0.5 to 3 cm for DCS and 0.5 to 6 cm for DRS. Black, flexible silicone material was used to tightly hold the fibers in place, and elastic straps were used to fix the probe around the muscle. Several optical switches were employed to switch the four wavelengths and six source positions consecutively. Two computers worked as control panels for DRS and DCS; they communicated via digital I/O lines. The sampling time for the DCS measurement was 1.5 s. A complete frame of data, cycling through all source-detector pairs, was acquired in 2.5 s.

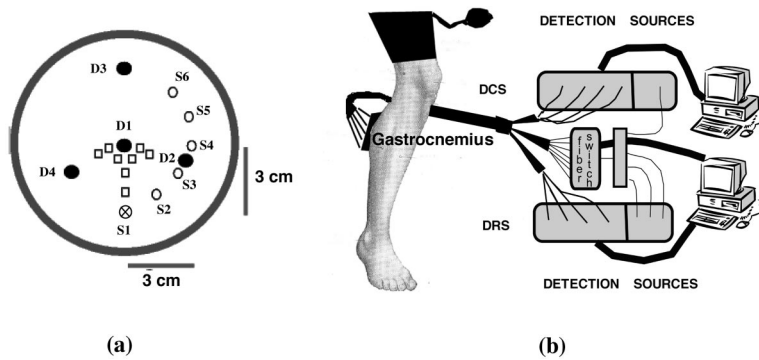


Fig. 1 A schematic of the hybrid instrument (panel b) combining diffuse correlation spectroscopy (DCS) and diffuse reflectance spectroscopy (DRS) for measuring of blood flow and oxygenation. The probe head (panel a) used in this study has eight DCS detector fibers (empty squares) at the periphery of concentric circles around one DCS source fiber (cross, S1); it also has four DRS detector fibers (solid circles, D1 to D4) with six source fibers (empty circles, S1 to S6) arranged on a 3-cm radius circle. The sampling time for a complete set of data was 2.5 s.

2.3 Data Analysis

Our experiments derive tissue physiological properties such as hemoglobin concentration and blood oxygen saturation from DRS measurements, and derive blood flow from DCS measurements. Information about changes in tissue oxygen metabolism rely on a simple model that utilizes the parameters we measure directly.

DRS for blood oxygenation. The procedures to obtain time curves of (S_tO_2) and THC have been described previously.^{19,20} Briefly, we model the tissue as a semi-infinite homogeneous medium and use a wavelength-dependent semi-infinite analytical solution to the photon diffusion equation to fit for the bulk optical properties of the underlying tissue. The bulk optical properties of muscle all derived from data at large source-detector separations (i.e., >1 cm). The optical properties of the tissue are characterized by an absorption coefficient μ_a and a reduced scattering coefficient μ'_s . The probe design shown in Fig. 1(a) exploits the symmetry of source and detector positions in order to calibrate the source and detector coupling coefficients (e.g., tissue-fiber coupling, light transmission efficiency, detector gain). For calibration, we first assume the underlying tissue to be homogeneous. Since only *relative* amplitudes and phases are of concern, we next assume the coupling coefficients for D1 and S1 to be unity and employ the symmetry to find coefficients for other sources and detectors. For example, D1 is at the center of all sources and is thus used to calibrate the source coefficients relative to S1. S1 is then used to calibrate D2 and D4 relative to D1 since they are equidistant. Similarly, S5 is used to calibrate D3 relative to D1. The coupling coefficients are multiplicative for amplitude and additive for phase. We have validated this procedure on phantoms and obtained good agreement with theoretical predictions over a large range of optical properties. It has also worked well for amplitude signals in tissues but since the phase signal is more sensitive and more noisy (in part, due to large dynamic range of our measurements), we ignore phase from our analysis. This analysis, therefore, required knowledge of the reduced scattering coefficient, which we assumed. Our model assumes a baseline reduced scattering coefficient, $\mu'_s = 5 \text{ cm}^{-1}$ at 785 nm.^{3,27} The influence of this approximation on the extracted relative changes will be discussed.

The wavelength-dependent μ_a is decomposed into contributions from different tissue chromophores, i.e., $\mu_a(\lambda) = \sum_i \epsilon_i(\lambda) c_i$. The sum is over all relevant tissue chromophores; $\epsilon_i(\lambda)$ is the extinction coefficient as a function of wavelength for the i 'th chromophore, and c_i is the unknown concentration of the i 'th chromophore. Oxy- and deoxy-hemoglobin and water are the most significant tissue absorbers in the NIR. Combinations of these parameters yield total hemoglobin concentration ($\text{THC} = C_{\text{Hb}} + C_{\text{HbO}_2}$) and blood oxygen saturation $\{S_tO_2 = [C_{\text{HbO}_2} / (C_{\text{Hb}} + C_{\text{HbO}_2})] \times 100\}$. Here C_{HbO_2} and C_{Hb} are tissue oxy- and deoxy-hemoglobin concentrations, respectively.

DCS for relative blood flow. Speckle fluctuations of the diffuse light are sensitive to the motions of tissue scatterers such as red blood cells. The quantity containing this information is the electric field $(E(r, t))$. The electric field temporal autocorrelation function, $G_1(r, \tau) = \langle E(r, t) E^*(r, t + \tau) \rangle$, or its Fourier transform is explicitly related to the motion of the scatterers (e.g., red blood cells). Here the angle brackets $\langle \rangle$ denote averages over time and τ is called the correlation delay time. A continuous-wave laser with a long coherence length and a single photon counting APD are needed for DCS measurements. A special piece of equipment called an autocorrelator takes the APD output and uses photon arrival times to compute the light intensity autocorrelation function. From the normalized intensity autocorrelation function, we calculate the normalized diffuse electric field temporal autocorrelation function $g_1(r, \tau) = G_1(r, \tau) / \langle E(r, t) E^*(r, t) \rangle$; $G_1(r, \tau)$ satisfies the correlation diffusion equation in highly scattering media.^{22,28-30} The exact form of the correlation diffusion equation depends on the nature and heterogeneity of the particle motion. For the important case of random flow in the tissue vasculature, the mean-square displacement, $\langle \Delta r^2(\tau) \rangle$, of the scattering particles (e.g., blood cells) in time τ is $\langle \Delta r^2(\tau) \rangle = \langle V^2 \rangle \tau^2$. Here $\langle V^2 \rangle$ is the second moment of the cell velocity distribution. In this case the normalized correlation function $g_1(r, \tau)$ will decay at early time approximately exponentially in τ . Its decay depends on a parameter α (proportional to the tissue blood volume fraction), and on the mean-square displacement of the blood cells. Relative changes in $\sqrt{\langle V^2 \rangle}$ are correlated with relative changes in tis-

sue blood flow. In this study only *relative* blood flow is reported. A detailed description of these concepts and approximations can be found in Refs. 19 and 20.

DCS data at the same source-detector separations were averaged. The bulk muscle flow responses derived in this paper utilize only data from large source-detector separations (i.e., >1 cm).

Blood oxygenation and flow in different layers. The tissues we investigate are layered (skin, adipose tissue, and muscle). From diffusion theory, the maximum penetration depth of diffuse light in tissue depends on tissue optical properties and source-detector separation. Therefore, specific source-detector separation pairs predominately provide the information about particular tissue layers (see also Sec. 4). To study the responses from different layers, flow properties were extracted from sets of source-detector pairs with the same separation. Similarly, DRS data from sets of source-detector pairs with the same separation was normalized by its baseline value to derive the relative change of tissue blood oxygen saturation (ΔS_tO_2) for the corresponding layer. Absolute baseline S_tO_2 was estimated from our multi-distance DRS measurement (described above).

Influence of μ'_s approximation. In the calculation of blood oxygenation and flow, it is possible the assumed baseline value of the scattering coefficient μ'_s may influence calculation accuracy. This influence was investigated by varying the assumed value of μ'_s and then comparing the relative changes of oxygenation and flow. We found empirically that a $\sim 100\%$ change in baseline μ'_s introduced less than a 5% error in the calculated *relative* change of chromophore concentration and oxygen saturation. The error induced in the calculated rBF was less than 1%.

Tissue oxygen consumption. We model tissue oxygen consumption (VO_2) in muscle in the same manner as is done with the cerebral metabolic rate of oxygen consumption.^{19,31} In steady-state, VO_2 depends on the difference in oxygen concentration across the vasculature (i.e., arteriole minus venule) times the blood flow rate: $VO_2 = (OEF) \times (BF) \times ([O_2]_a)$. This equation is sometimes referred to as Fick's law.^{16,31} Here $[O_2]_a$ is the arterial oxygen concentration, OEF is the tissue oxygen extraction fraction defined as $([O_2]_a - [O_2]_v) / ([O_2]_a)$, subscripts v and a denote venous and arterial sides, and BF is tissue blood flow. This general equation is used in the analysis of many oxygen metabolism problems, particularly those associated with activation in brain^{19,20} and muscle.^{16,27,32,33}

For relative changes in these variables we define: $rBF = BF / BF_{baseline}$, $rOEF = OEF / OEF_{baseline}$, and $rVO_2 = VO_2 / VO_{2baseline}$. Assuming the arterial oxygen concentration, $[O_2]_a$, does not change, the relative change in muscle oxygen consumption is: $rVO_2 = rOEF \times rBF$. Here r denotes relative change. The oxygen extraction fraction, OEF, is related to tissue blood oxygen saturation: $OEF = (S_aO_2 - S_tO_2) / (\gamma \times S_aO_2)$. Here S_aO_2 and S_tO_2 are arterial and tissue saturations, respectively, and γ indicates percentage of blood volume contained in the venous component of the vascular system.^{19,31}

Our DCS measurement enables us to determine rBF. Our DRS measurement enables us to determine S_tO_2 . S_aO_2 is not measured by DRS, but is assumed to stay constant near unity.

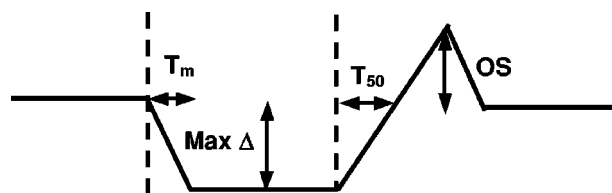


Fig. 2 Characterization of the flow response during cuff occlusion. Variables used to describe the hemodynamic response include: maximal change (Max Δ), time constant from manipulation onset to maximal response [T_m (s)], recovery half-time [T_{50} (s)], and amount of overshoot [OS (Δ)]. Vertical lines indicate the beginning and end of the occlusion.

This assumption was verified experimentally; an S_aO_2 of 98% was found during mild plantar flexion exercise.³⁴ Thus, we can obtain OEF directly from the measured S_tO_2 . Notice further, if we assume γ remains constant, then this compartment parameter divides out of our estimate of rOEF. The influence of this assumption about γ is discussed in Sec. 4.

Characterization of responses. Time traces for tissue oxygen saturation [S_tO_2 (%)], total hemoglobin concentration [THC (μM)], and relative blood flow [rBF (%)] are derived for both cuff occlusion and exercise. A time curve for relative tissue oxygen consumption [rVO_2 (%)] is then calculated and presented for plantar flexion exercise; According to ³¹P-nuclear magnetic resonance spectroscopy measurements, VO_2 does not change ($rVO_2 = 1$) throughout a short period of arterial occlusion (<5 min),³⁵ and neither does rOEF. We assign 100% as the baseline value for all relative variables (e.g., rBF, rOEF, and rVO_2).

In order to evaluate the measurement accuracy we assume signal fluctuations as measured at rest are due to measurement errors. Thus a percent error is estimated by the standard deviation of 50 measurement time points at rest, divided by the mean of these values.

To characterize hemodynamic responses, mean and standard deviation are tabulated for maximal change (Max Δ), time constant from manipulation onset to maximal response [T_m (sec)], recovery half-time [T_{50} (sec)] and amount of overshoot [OS (Δ)]. Figure 2 shows an example for characterization of the blood flow response (rBF) during a cuff occlusion in terms of these variables. Other variables (e.g., S_tO_2 , THC, and/or rOEF, rVO_2) during cuff occlusion and during exercise are characterized in the same manner. Significant differences were identified by a paired t-test. The criterion for significance was $p < 0.05$.

3 Results

3.1 Tissue Layer Responses

Figure 3 shows the typical relative blood flow (rBF) and tissue oxygen saturation (S_tO_2) responses during leg arterial occlusion from different source-detector pairs measured on a healthy individual. The source-detector separations were 0.5, 1.5, 3, 4, and 5 cm for DRS [only some of data are shown in Fig. 3(b) for clarity], and 0.5, 1, 2, and 3 cm for DCS respectively. Figure 4(a) shows the relationship between the magnitude of *reactive hyperemia* (i.e., the blood flow overshoot following cuff occlusion) and source-detector separation

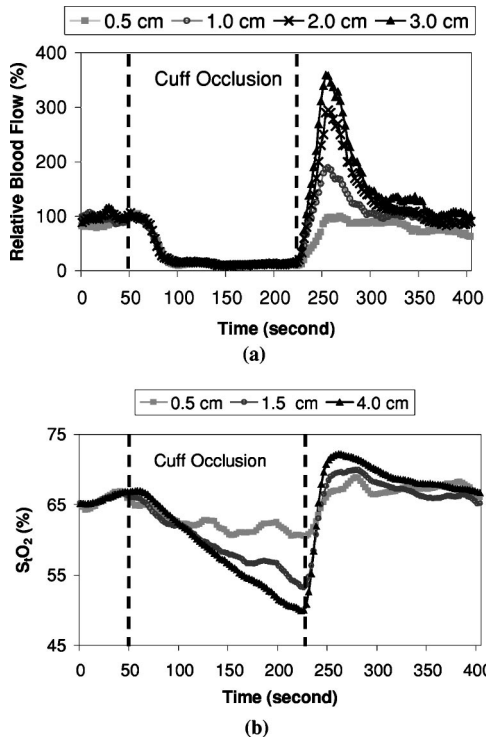


Fig. 3 Representative time curves of relative blood flow (panel a) and tissue oxygen saturation (panel b) during arterial cuff occlusion from different source-detector pairs measured on a healthy leg. The source-detector separations shown in the figure are 0.5, 1, 2, and 3 cm for DCS, 0.5, 1.5, and 4.0 cm for DRS respectively. Vertical lines indicate the beginning and end of the occlusion. The stronger *reactive hyperemia* after the release of occlusion, and deoxygenation during occlusion were derived from source-detector pairs with large separations, i.e., 2 and 3 cm for DCS, 1.5 and 4 cm for DRS, respectively.

averaged over five healthy subjects ($n=5$). Figure 4(b) shows the relationship between S_tO_2 maximum decrease during occlusion versus source-detector separation ($n=5$). Notice, in this layer analysis the transverse dimension is assumed homogeneous. We average over the different transverse positions when deriving a layer response (see also Section 2), and the error bars that subsume these effects are given in Figure 4. The hemodynamic responses derived from source-detector pairs with large separations (≥ 2 cm) for both legs and arms were significantly stronger than these from the shortest source-detector separations (0.5 cm). We believe these stronger responses are mainly from the muscle layer (see Section 4). Therefore signals derived from larger source-detector separations (> 1 cm) are assigned to the muscle and are used in our analysis.

3.2 Cuff Occlusion Response

Table 1 lists the hemodynamic responses in cuff occlusions from ten healthy volunteers ($n=10$) and one PAD patient ($n=1$). S_tO_2 (%) and THC (μM) were fit using data derived from source-detector separations of 3 to 5 cm; rBF (%) was calculated by averaging signals from source-detector separations of 2 cm and 3 cm in different locations.

For the healthy volunteers, cuff occlusion of the leg flexor and arm flexor muscles produced a similar response. The

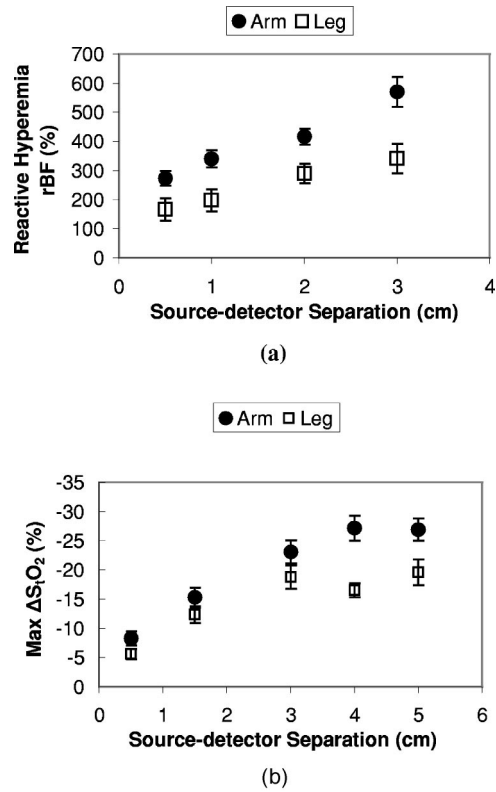


Fig. 4 Relationships between hemodynamic response and source-detector separation averaged over five healthy subjects ($n=5$). Values are means \pm standard errors. Vertical axis in panel (a) refers to the magnitude of *reactive hyperemia* after release of cuff occlusion, while the vertical axis in panel (b) refers to S_tO_2 maximum decrease during occlusion. The magnitudes of *reactive hyperemia* (shown in panel a) derived from source-detector pairs with large separations (≥ 2 cm) for both legs (empty square) and arms (solid circle) were significantly higher ($p<0.05$) than those from the shortest source-detector separations (0.5 cm) respectively. The S_tO_2 responses (shown in panel b) derived from large separations (≥ 1.5 cm) for both legs and arms were significantly stronger ($p<0.01$) than those from the shortest separations (0.5 cm), respectively.

rapid increase of cuff pressure induced a rapid and substantial decrease in rBF: Max $\Delta rBF = -90.0 \pm 2.4\%$ for leg and Max $\Delta rBF = -90.3 \pm 3.8\%$ for arm (baseline value = 100%). There was also a gradual decrease in S_tO_2 throughout the arterial occlusion. The maximal decrease of S_tO_2 occurred at the end of the 3-min cuff occlusion: Max $\Delta S_tO_2 = -16.4 \pm 4.4\%$ for leg and Max $\Delta S_tO_2 = -25.1 \pm 8.2\%$ for arm respectively. A constant minimal value of S_tO_2 (plateau) was observed after ~ 5 min from separate measurements not shown here ($n=2$, 10-min occlusion).

The typical reactive hyperemia following the release of occlusion (Max $\Delta rBF = 311.4 \pm 90.8\%$ for leg and Max $\Delta rBF = 445.1 \pm 194.1\%$ for arm) was much higher than the oxygen peak overshoot (Max $\Delta S_tO_2 = 3.8 \pm 1.7\%$ for leg and Max $\Delta S_tO_2 = 11.4 \pm 5.0\%$ for arm).

During cuff occlusion THC was generally unchanged. There was, however, variation between trials. We believe this variation was primarily due to delays between venous occlusion and full arterial occlusion during both inflation and deflation which leads to trapping of blood in the capillaries.

Table 1 Responses in cuff occlusions from ten healthy volunteers and one PAD patient. Time to reach maximal change (T_m), maximal change (Max Δ), recovery half-time (T_{50}), and hyperemic overshoot (OS) are shown for S_tO_2 (%), THC (μM), and rBF (%). Means \pm SD are reported.

Parameters	Subjects	T_m (s)	Max Δ	T_{50} (s)	OS (Δ)
Leg occlusion					
S_tO_2 (%)	Healthy	177.1 \pm 20.7	-16.4 \pm 4.4	33.7 \pm 26.0	3.8 \pm 1.7
	PAD	180.0	-15.0	96.0*	3.0
THC (μM)	Healthy	88.1 \pm 81.9	-1.8 \pm 5.9	16.2 \pm 18.3	2.8 \pm 3.1
	PAD	25.0	-10.0	36.0	5.0
rBF (%)	Healthy	51.0 \pm 11.5	-90.0 \pm 2.4	25.6 \pm 14.5	311.4 \pm 90.8
	PAD	60.0	-93.0	90.0*	165.0*
Arm occlusion					
S_tO_2 (%)	Healthy	174.7 \pm 15.3	-25.1 \pm 8.2	19.4 \pm 15.2	11.4 \pm 5.0
	PAD	180.0	-23.0	23.0	10.0
THC (μM)	Healthy	46.6 \pm 61.2	-1.4 \pm 6.4	13.6 \pm 7.3	8.6 \pm 5.0
	PAD	111.0	-16.0	20.0	22.0
rBF (%)	Healthy	14.0 \pm 7.4	-90.3 \pm 3.8	11.3 \pm 6.1	445.1 \pm 194.1
	PAD	11.0	-92.0	12.0	450.0

*Substantially different, healthy volunteers vs. the PAD patient.

The hemodynamic response trends in the PAD patient were similar to those of the healthy volunteers (data are not shown here), and different responses were not found in the arm muscles of healthy controls compared to the patient. However, in the patient leg muscle, the relative magnitude of reactive hyperemia was $\sim 1/2$ of the controls and the recovery half-times of both S_tO_2 and rBF after occlusion were about triple those of the controls (see Table 1).

3.3 Plantar Flexion Exercise Response

Figure 5 shows the typical time curves of rBF & rVO_2 (panel a, b), and S_tO_2 & THC (panel c, d) during plantar flexion exercise from a healthy individual (panel a, c) and a PAD patient (panel b, d). rBF during exercise did not exhibit different phases of the muscle activity (contraction and relaxation) due to the comparatively long sampling time (2.5 s). A separate trial with higher temporal resolution (~ 1 Hz), achieved by changing the measurement duration for DCS and using only one source position for DCS and DRS measurements, exhibited flow oscillations that correlated well with muscle contraction and relaxation (see Fig. 6).

Table 2 summarizes the hemodynamic responses during exercise from ten healthy volunteers ($n=10$) and one PAD patient ($n=1$). The healthy muscle responses showed variation among subjects. After the exercise began, rVO_2 increased ~ 7 fold ($694.5 \pm 176.5\%$) within a short time (14.9 ± 8.1 s) while rOEF also increased ~ 1.5 fold ($146.6 \pm 56.8\%$) in 29.4 ± 8.7 s. To meet the increase in oxygen demand, rBF increased rapidly and reached a maximum ($473.7 \pm 138.6\%$) in the same short time (14.9 ± 8.1 s). This increase in flow during exercise is termed *active hyperemia*. The greatest discrepancy between rBF and rVO_2 occurred for ~ 15 s demonstrating the maximum mismatch between oxygen delivery and oxygen demand. THC decreased and reached a minimum (Max Δ THC = $-17.6 \pm 9.9 \mu M$) almost as fast as rBF (18.3 ± 9.6 s), while S_tO_2 also decreased rapidly and reached a minimum (Max Δ S_tO_2 = $-17.1 \pm 7.9\%$) in 29.4 ± 8.7 s. After reaching a maximum or minimum, the variables fluctuated

randomly around their extremes. Once the exercise was stopped, rBF and rVO_2 recovered rapidly to their baseline values, whereas THC, S_tO_2 and rOEF recovered more slowly toward their baseline values. The recovery half-times (T_{50}) of rBF and rVO_2 after occlusion were too fast to be measured with our present temporal resolution (i.e., 2.5-s sampling time).

We were able to quantify these healthy responses repeatedly. In studies not shown here, we tested measurement repeatability on healthy individuals (two trials, $n=2$); the variation fell within the range shown in Table 1 and Table 2. A similar variation was observed between left/right arm/leg of healthy individuals.

The PAD patient and the healthy volunteers had similar dynamic response trends in the plantar flexion exercise (see Figure 5). However, the relative magnitudes of active hyperemia, THC, and rVO_2 during exercise in the diseased leg were half of the healthy controls, and the recovery half-time of S_tO_2 after exercise was double the controls (see Table 2 and Figure 5).

4 Discussion

In this section we first address the issue of adequate penetration of DCS and DRS for probing deep muscle tissue. We then discuss our observations of hemodynamic response in human muscle during arterial occlusion and plantar flexion exercise, and compare them with previous studies based on other technologies. We also discuss the myoglobin contributions to our NIRS measurements, and the influence of our model assumption on the calculation of rVO_2 .

4.1 Does Our Instrument Probe Deep Muscle Tissue?

DRS has been applied and validated in studies of deep muscle tissue and adipose tissue.³⁶⁻³⁸ DCS, however, has not been applied in muscle studies. We addressed the issue of adequate penetration by experimentally investigating tissue layer responses during cuff occlusion.

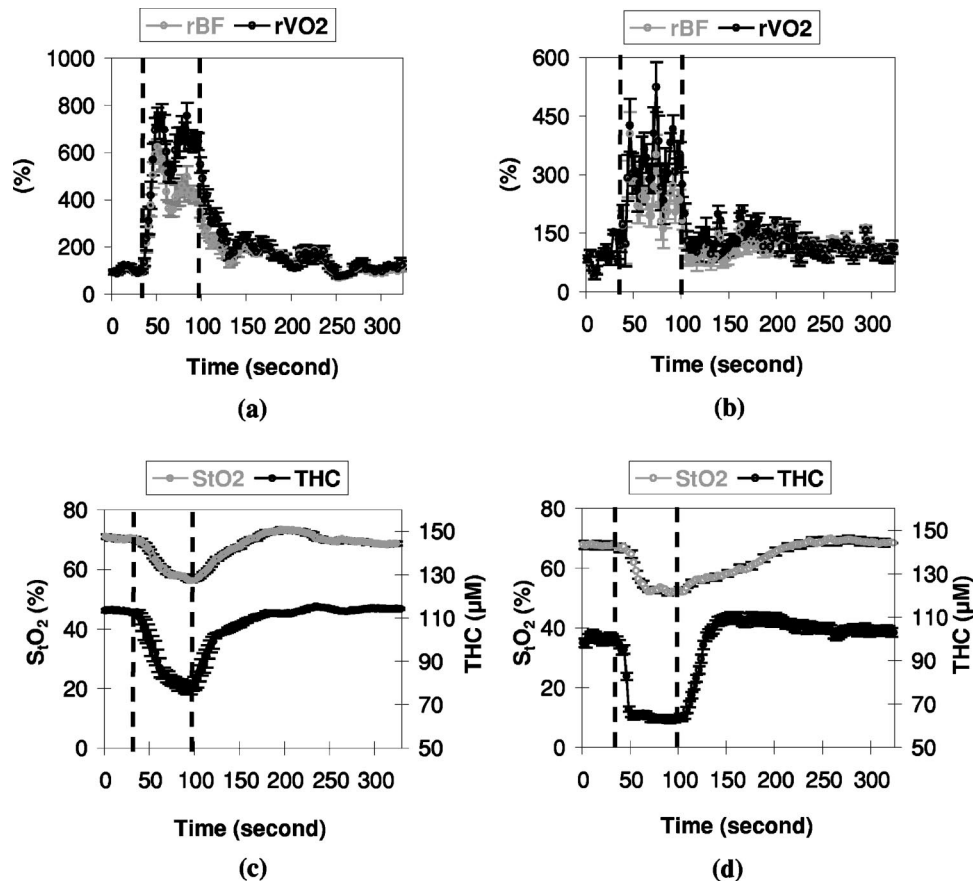


Fig. 5 Hemodynamic responses during one-minute plantar flexion exercise from a healthy individual (panel a, c) and a PAD patient (panel b, d). The time curves of rBF and rVO₂ (panel a, b), S_tO₂ and THC (panel c, d) are shown and the error bars are estimated by the standard deviation of 50 time points during the baseline converted to percent error (see text). Vertical lines indicate the beginning and end of the exercise. The sampling rate for a complete set of data was 0.4 Hz.

Skin and adipose tissue layers generally lie above muscle. According to the skinfold caliper, the thickness of the upper layers (skin and adipose tissues) above leg flexors and wrist flexors in our volunteer population were 5.5 ± 0.4 mm and 2.8 ± 0.6 mm respectively ($n=10$). From diffusion theory, light penetration depth depends on tissue optical properties

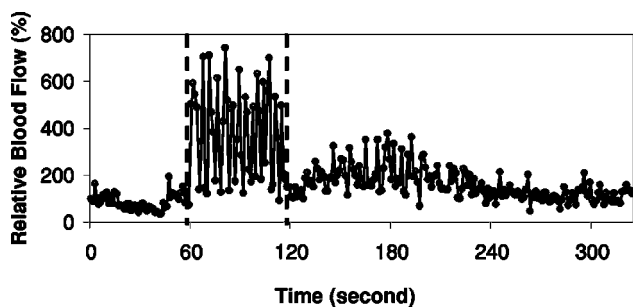


Fig. 6 Representative time curve of relative blood flow (rBF) during one-minute plantar flexion exercise from a healthy individual. Vertical lines indicate the beginning and end of the exercise. With the higher temporal resolution (~ 1 Hz), diffuse correlation spectroscopy (DCS) detects the two phases during rhythmical exercise: a decrease flow during muscle contraction and an increase flow during muscle relaxation.

and source-detector separation. Figure 7 displays a multi-layer tissue model and a simulated schematic of diffuse light penetration for the different source-detector separations. For simplicity, tissue was assumed homogeneous (tissue absorption coefficient $\mu_a = 0.1 \text{ cm}^{-1}$; reduced scattering coefficient $\mu'_s = 5 \text{ cm}^{-1}$). Semi-infinite, three-point Green's functions were used to simulate the photon path distribution in the tissue for each source-detector pair. The shaded areas define points, \vec{r} , such that the probability a photon leaves the source, arrives at the detector, and passes through \vec{r} is greater than 50%. Clearly, signals detected by source-detector pairs with separations of 2 cm and 3 cm derive mainly from the muscle layer, whereas signals from shorter separations are derived from upper layers. Note, however, even at large source-detector separations there is always some contribution to the signal from the overlaying tissue. In order to quantify the penetration depth of diffuse light, accurate knowledge of tissue optical properties, layer thickness, and multi-layer theoretical models are desirable.³⁶⁻³⁸ We avoided the complexities associated with measuring these variables by experimental calibration based on reactive hyperemia following arterial occlusion release.

Reactive hyperemia, following rapid release of arterial occlusion, is a transient increase in blood flow. The ability of an organ to display reactive hyperemia is related to its ability to

Table 2 Responses in plantar flexion exercise from ten healthy volunteers and one PAD patient. Time to reach maximal change (T_m), maximal change ($\text{Max } \Delta$), recovery half-time (T_{50}), and relative overshoot (OS) are shown for S_tO_2 (%), THC (μM), rBF (%), rOEF (%), and rVO_2 (%). Means \pm SD are reported. NA indicates that quantity is not measurable with the present temporal resolution (i.e., 2.5 s sampling time).

Parameters	Subjects	T_m (s)	Max Δ	T_{50} (s)	OS (Δ)
S_tO_2 (%)	Healthy	29.4 ± 8.7	-17.1 ± 7.9	36.7 ± 22.8	4.8 ± 3.6
	PAD	22.0	-12.3	70.0*	3.0
THC (μM)	Healthy	18.3 ± 9.6	-17.6 ± 9.9	23.7 ± 13.9	3.3 ± 3.9
	PAD	12.0	-32.8*	16.0	10.0
rBF (%)	Healthy	14.9 ± 8.1	473.7 ± 138.6	NA	-9.5 ± 19.5
	PAD	12.0	240.0*	NA	-10.0
rOEF (%)	Healthy	29.4 ± 8.7	146.6 ± 56.8	36.7 ± 22.8	-15.1 ± 12.8
	PAD	22.0	141	70.0*	-9
rVO_2 (%)	Healthy	14.9 ± 8.1	694.5 ± 176.5	NA	-7.5 ± 15.9
	PAD	12.0	338.4*	NA	-18

*Substantially different, healthy volunteers vs. the PAD patient.

auto-regulate.³⁹ Different organs display varying degrees of auto-regulatory behavior. For example, skeletal muscle shows moderate auto-regulation, while cutaneous microcirculation shows little or no auto-regulatory capacity.³⁹ Reactive hyperemia occurs because during the period of occlusion, tissue hypoxia and a buildup of vasodilator metabolites decrease vascular resistance. Both oxygen consumption and oxygen extraction are much lower in adipose tissue than muscle tissue.³⁵ The lower metabolism leads to a smaller accumulation of vasodilator metabolites during arterial occlusion in adipose tissue, thus inducing a lower magnitude of reactive hyperemia compared to muscle.

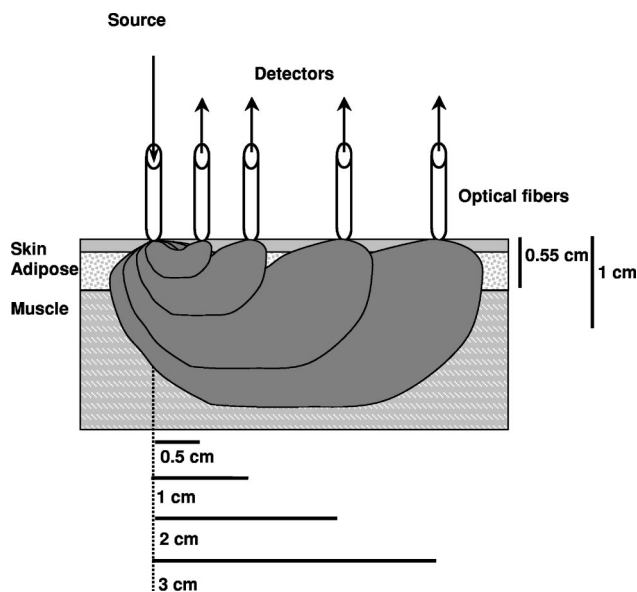


Fig. 7 A schematic of a multi-layer tissue model and the simplified presentation of diffuse light penetration in relation to the different source-detector separations. The thickness of upper layer (skin and adipose tissue), as measured by a skinfold caliper, is ~ 5.5 mm. The source-detector separations are 0.5, 1, 2, and 3 cm respectively. Clearly, the signals from the large separations of 2 cm and 3 cm derive mainly from the muscle tissue whereas signals from 0.5 cm and 1 cm are mainly from upper layers.

From Fig. 4(a), we see that the magnitudes of reactive hyperemia derived from source-detector separations of 2 cm and 3 cm are significantly higher than those from shorter separations. Taken together, the simulation results (see Fig. 7) and the measurements [see Fig. 4(a)], suggest the stronger hyperemic signals (from 2 cm and 3 cm separations) originate mainly from the strong auto-regulation of muscle tissue; the weaker responses (0.5 cm and 1 cm source-detector separations) represent the response of cutaneous tissues.

A lower magnitude of reactive hyperemia was also found from human wrist skin by use of laser Doppler flowmetry.¹⁰ Binggeli et al.¹⁰ found that after 4.5-min arterial occlusion, hyperemic skin blood flow increased ~ 2 fold, which is in reasonable agreement with the 1.7 ± 0.9 fold increases found from superficial layers (0.5 cm separation) in this study. Similarly, the maximum changes of S_tO_2 during arterial occlusion derived from source-detector separations of 3 to 5 cm are much higher than those from 0.5 cm and 1 cm separations [see Fig. 4(b)]. Again this observation is consistent with our expectation for the responses of muscle layers.

The substantially smaller variations of hemodynamic responses ($p > 0.05$) detected at larger separations (≥ 2 cm) are probably due to the different fractions of muscle tissue probed. For example, a source-detector separation of 3 cm probes a larger fraction of muscle tissue than that of the 2 cm separation (see Fig. 7), and gives a slightly stronger response (see Fig. 4).

In total these findings suggest that DRS and DCS probe through the upper tissue layers into the muscle tissue. In practice it is critical to choose source-detector separations in the appropriate range to discriminate muscle responses from over-layer responses.

4.2 Healthy Subjects Responses

The hemodynamic responses of healthy muscle tissues in ten healthy volunteers, have demonstrated comparable and repeatable variations during hemodynamic perturbations. At the onset of the arterial occlusion, blood flow rapidly falls to a minimum value ($\sim 10\%$ of the baseline value) [see Fig. 3(a)]. This minimum measurable blood flow during cuff occlusion is the so-called “biological zero.”⁴⁰ Muscle oxygen saturation

(S_tO_2) on the other hand, decreases gradually [see Fig. 3(b)] during the occlusion, as a result of continuous oxygen consumption in tissues and minimal blood flow (oxygen delivery). The declining rate of muscle oxygenation reflects the level of muscle oxygen consumption at rest.³⁵ When the occlusion is released, there is a reactive hyperemia because of the auto-regulation (vasodilation) of muscle vasculature in response to metabolites (e.g., CO_2 , H^+ , lactate) created during ischemia. During the hyperemia, oxygen is replenished and the metabolic stimulus for vasodilation is washed out, causing vasoconstriction. Thus blood flow and oxygen return to their normal resting levels.

Characterization of dynamic exercise is more difficult because of its complexity and the speed of metabolic mechanisms. Exercise consumes large amounts of energy and therefore requires delivery of considerable amounts of oxygen and substrate, as well as the removal of waste metabolites (e.g., CO_2 , H^+ , lactate). The intrinsic auto-regulation ability in muscle vasculature increases blood flow to meet the increased need for delivery and removal.

Mean blood flow increases during plantar flexion exercise (see Fig. 5). However, if blood flow is measured without averaging, the flow will be seen in two phases—a decrease flow during contraction and an increase flow during relaxation.^{39,41} With higher temporal resolution (~ 1 Hz), DCS captures these two phases (see Fig. 6). The increased blood volume during muscle relaxation mainly increases blood in the capillary component, i.e., the previously “clamped” capillaries open (*vascular recruitment*). In contrast, the muscle contraction mainly compresses the venous component of the vascular tree propelling blood toward the heart.⁴² Notice further that the comparatively larger fluctuations following exercise in both muscle blood flow and oxygen consumption are connected with the recovery period of muscle blood oxygen saturation (S_tO_2) (see Fig. 5 and Fig. 6).

The magnitude of the active hyperemia (rBF) found in this study was closely related to the increase in muscle oxygen consumption (rVO₂) throughout the period of exercise; however, the average increases were quite different (Fig. 5 and Table 2). The average increase in blood flow at the transition from rest to the exercise was ~ 4.7 fold whereas the average increase in rVO₂ was ~ 7 fold. The increase in rBF was significantly lower than the increase in rVO₂ ($p < 0.05$). Thus a decrease in muscle oxygenation saturation (S_tO_2) was produced. This observation suggests that increased oxygen demand cannot be completely met by an increase in blood flow. Our finding is in agreement with the results obtained by Beekvelt et al.,⁴³ who found in the active flexor digitorum superficialis (FDS) that increased demand for oxygen is mostly met by an increase in oxygen extraction. The mismatch between blood supply and oxygen demand is an important factor in determining the cellular depletion of energetic metabolites,⁴⁴ and the magnitude of active hyperemia during exercise is believed to be related to the metabolite-induced vascular response. Thus the ability to track muscle flow and energy demand may be very useful for assessment in the clinic.

4.3 The Patient with Peripheral Arterial Disease (PAD)

In this section we discuss our observations of the single PAD patient; we note, however, that our small sample size qualifies our conclusions. The different responses of healthy volunteers and the PAD patient are listed in Table 1 and Table 2. Our observation of substantially longer recovery half-times of S_tO_2 ($T_{50} = 96$ s for cuff occlusion and $T_{50} = 70$ s for exercise) in the diseased leg were consistent with previous studies.^{3,45} A longer recovery half-time of rBF ($T_{50} = 90$ s) was also found in the diseased leg after release of cuff occlusion. While the longer recovery times are not surprising, the magnitude of active hyperemia (rBF) and rVO₂ during the exercise in the diseased leg were only half of those in healthy volunteers (see Table 2). A similar observation was made about the magnitude of reactive hyperemia in the diseased leg during occlusion (see Table 1). These weaker flow responses of diseased tissue may have important consequences affecting the oxygen delivery and ability to support muscle metabolism.

Less blood flow delivery during exercise in the diseased leg leads to a greater decrease of tissue THC as well (see Table 2). In contrast, all responses from the patient arm were within the normal range; the patient arm also had no obvious symptoms. Using NIRS or PET, Wolf et al.,¹⁸ Burchert et al.,¹³ and Paunescu²⁷ independently found no significant difference in blood flow and oxygen consumption at rest between PAD patients and healthy subjects. Although our study has no statistical power for the patients at the moment, our work is potentially indicative of the need for measurement of the dynamic responses during exercise or cuff occlusion.

4.4 Myoglobin Contribution to the NIRS Measurements

An important issue in muscle studies centers around the role of myoglobin (Mb) for oxygen regulation. The presence of myoglobin does not influence our DCS blood flow measurement, because DCS is sensitive to the motion of blood cells and myoglobin is an oxygen storage protein that remains static in muscle cells. However, the near-infrared DRS signal can be “contaminated” by myoglobin, since myoglobin and hemoglobin (Hb) have very similar optical spectra.

Most of the optical signals in our study originate from hemoglobin because of the following. (1) Within a given volume of muscle, the concentration of Hb is about 1.5 times higher than that of Mb, and Hb has four oxygen binding sites compared to the one binding site of Mb. Therefore we estimate the Mb mass affects less than 20% of oxygen response.^{14,35} (2) During suprasystolic cuff occlusion, the deoxy-Mb signal as measured by ¹H MRS appeared after 4 min.⁴⁶ Conversely, tissue oxygen saturation (S_tO_2) during our 3-min cuff occlusion decreased immediately following occlusion and reached a maximum at the end of occlusion. Thus this gradual decrease of S_tO_2 during occlusion must due to the hemoglobin deoxygenation. (3) In a study of 4-min peak plantar flexion, as measured by the continuous wave NIRS and ¹H MRS, Mancini et al. found that NIRS absorption in the gastrocnemius muscle is primarily derived from deoxygenated hemoglobin and not myoglobin.⁴⁷ Their protocol is similar to ours except the exercise period (4 min) is longer than ours (1 min). Therefore, during our relatively mild 3-min cuff occlu-

sion and 1-min plantar flexion exercises we expect myoglobin to remain mostly oxygenated due to their higher affinity for oxygen compared to hemoglobin.

Our study is not designed to resolve the Hb-Mb issue. Therefore, the oxygenation changes presented here are more accurately viewed as a combination of hemoglobin and myoglobin with a relatively low contribution (<20%) from myoglobin. The effect of this contribution on the calculation of the changes in muscle oxygen consumption can be the subject of future studies where measures of myoglobin and metabolism through magnetic resonance spectroscopic methods¹² will be compared to optical results.

4.5 Comparison of Responses with Other Studies

Blood oxygenation (DRS). The observed maximum decrease of S_tO_2 at the end of the 3-min arterial cuff occlusion (see Table 1) is in good agreement with other published results in the arm^{48,49} and leg.³ This is not surprising since similar NIRS technology and similar source-detector separations (2 to 5 cm) were used. Although the occlusion duration of 5 to 10 min applied in these early studies^{3,48,49} was longer than ours (3 min), duration does not influence the comparison of maximum decreases of S_tO_2 at the 3-min time point. Furthermore, as mentioned before, in a subset of subjects ($n=2$) we observed a constant minimal value of S_tO_2 (plateau) after 5 min following occlusion, consistent with the literature.

There are only a few published studies using plantar flexion exercise as the clinical protocol to study the blood oxygenation in humans,^{34,50,51} and some of them did not report the absolute change of S_tO_2 .^{50,51} Quaresima et al.³⁴ used NIRS with a protocol of 40–80 plantar flexion/min in a supine position. They reported S_tO_2 of medial gastrocnemius began to decrease substantially from a baseline value of 69% about 15 s after the onset of exercise, reaching a minimal value (~30%) about 15 s later; it recovered to the baseline value 32 to 45 s after the end of the exercise. The trend, baseline value, and temporal responses (T_m and T_{50}) of S_tO_2 are in good agreement with our observations shown in Fig. 5 and Table 2. The maximal change of S_tO_2 ($\Delta S_tO_2 \approx -40\%$) during exercise was approximately two times larger than our observations ($-17.1 \pm 7.9\%$, $n=10$), and this difference is attributable to the different intensity of the exercise affecting the response. Other factors could also contribute to this difference, including age and gender of the subjects, and methodology.

Blood flow (DCS). Many noninvasive techniques have been applied to study perfusion changes in human skeletal muscle during reactive hyperemia. Doppler ultrasound imaging measured a 3 to 6 fold peak hyperemic flow after 2 min of forearm occlusion,^{7,8} which compares well to the ~4.5 fold reactive hyperemia found by our DCS in arm occlusion (see Table 1).

Both conventional venous occlusion plethysmography⁶ and MRS plethysmography^{52,53} present mean reperfusion peaks of 25–35 ml · 100 ml⁻¹ · min⁻¹ after 3 to 5 min forearm or calf arterial occlusion, and mean muscle perfusion at rest in the range of 3–5 ml · 100 ml⁻¹ · min⁻¹.^{6,52,53} This is approximately equivalent to a 7.5 fold (i.e., a range of 5–12) flow increase relative to the baseline, and approximately 2 times higher than the 3.8 fold (i.e., a range of 3.1–4.5) reactive hyperemia found in our study (see Table 1). Other studies also

found that plethysmographic flow was 2–3 times higher than the NIRS flow.^{43,44} Beekvelt et al. hypothesized a methodological difference exists between these two techniques.⁴³ Plethysmography reflects a total limb flow which contains blood coming from skeletal muscle, cutaneous tissues, bone, and tendons and might thus lead to a higher plethysmographic flow. In contrast, NIRS reflects only the local flow in the region of interest and primarily monitors small vessels (i.e., arterioles, capillaries, venules). Small vessels have lower hematocrit compared to big vessels, because hematocrit decreases with the decrease of the diameter of vessels. For example, in capillaries the hematocrit is lowest, about 25% lower than in whole body.²⁷ Lower hematocrit in small vessels results in a lower NIRS flow.⁴³

T_1 based MRI of blood reperfusion on the basis of arterial spin labeling (ASL) was found to be in good agreement with the established standards, such as PET and radioactive microsphere measurements.⁵⁴ Since muscle perfusion at rest is below the detection threshold of T_1 based MRI, the plethysmographic flow at rest was generally used as baseline to estimate the relative peak reperfusion.⁵⁴ However, this estimation may introduce large overestimates in the calculation of relative peak reperfusion, since plethysmographic flow is 3.8 times lower than the T_1 based MRI flow.^{52,53} Thus, we do not compare our relative DCS flow to MRI flow.

To our knowledge there have been no reports of tissue oxygen consumption (rVO_2) during plantar flexion using the same exercise protocol as ours. Thus it is impossible to compare our rVO_2 measurements with other research.

4.6 Modeling Assumptions for Relative Oxygen Consumption (rVO_2)

One assumption made in the calculation of rVO_2 was that vascular compartmentalization, γ , does not change. This assumption may not be true throughout exercise, since the percentage of blood contained in the venous component can change due to exercise. Error in rVO_2 will arise from different γ , before and during exercise. At rest, before exercise, the greatest blood volume resides in the venous vasculature, where normally 65–70% of the blood volume is found.⁴¹ Accordingly we assume $\gamma_{rest} \cong 67.5\%$. During exercise, muscle is very effective in returning blood to the heart by compression of venules and veins. Thus total blood volume in muscle decreases due to muscular compression. We found in this study that THC decreased during exercise by ~15% from a baseline of ~115 μM (see Fig. 5 and Table 2). THC reflects blood volume. Thus we may assume a ~15% decrease in total blood volume during exercise. For simplicity, we further assume this ~15% decrease in total blood volume is due to a decrease in venous vasculature. We then can estimate the γ during exercise: $\gamma_{exercise} \cong 61.8\%$. Overall, exercise induced a decrease of γ from ~67.5% to ~61.8%.

A decrease in γ during exercise compared to rest leads to an overestimate of rOEF by a factor, $(\gamma_{rest}/\gamma_{exercise} - 1) \times 100 = 9.2\%$. The ~9.2% overestimate of rOEF will lead in turn to a ~9.2% overestimate of rVO_2 . Considering the several fold changes of rVO_2 during exercise (see Table 2), this overestimate of rVO_2 may be considered unimportant.

The metabolic responses (rVO_2), as measured by our optical method, require more validation studies based on the

established techniques, such as MRS which can measure metabolic responses directly.¹² Taken together the unresolved issues described above suggest that our calculation is better regarded as an index of rVO_2 rather than an absolute measure.

4.7 Conclusions

Diffuse correlation spectroscopy (DCS) has been shown in this study to penetrate through layers of upper tissues to muscle tissue. This technique can therefore give accurate measurements of blood flow in the muscle capillary bed compared to plethysmography, because it is much less affected by blood flow from the surrounding tissues (e.g., cutaneous tissues, bone, tendons). Unlike venous occlusion NIRS and plethysmography for flow measurements, DCS does not interrupt the blood flow during measurement and is simple to perform.

The combination of DCS and diffuse reflectance spectroscopy (DRS) has allowed us to use both optical methods non-invasively and continuously, to measure relative blood flow (rBF), blood oxygen saturation (S_tO_2) and total hemoglobin concentration (THC) in deep muscle tissues under rest, during mild exercise and during extreme cuff occlusion. These hemodynamic parameters permit an estimation of the relative muscle oxygen consumption (rVO_2). Our hybrid instrumentation used in this study is portable, inexpensive, and safe for longitudinal studies. It has potential to become a clinical routine examination tool supplementary to MRS/MRI or PET.

Measurements on healthy volunteers ($n = 10$) allowed us to quantify healthy muscle responses (e.g., reactive hyperemia, active hyperemia, mismatch between blood supply and oxygen demand, recovery half-time), which were consistent with known physiology. Muscle responses have large variation and are reported to be heterogeneous in different locations.¹⁸ Pilot studies on a single PAD patient suggest we are able to distinguish features differentiating normal and diseased responses, but while these observations are encouraging, they cannot be extrapolated broadly until more statistically significant sample sizes are employed. Multi-parameter dynamic measurements such as these are essential for the assessment of disease and for evaluating of healthy muscle oxidative metabolism. Such information has potential to improve diagnostic and treatment options for PAD patients.

Acknowledgments

The authors acknowledge useful discussions with T. Chance, S. Nioka, J. Im, and T. Floyd. E. R. Mohler was supported in part through a grant from the Juvenile Diabetes Research Foundation. B. Chance acknowledges support from NIH5-R01-HL44125-15. A. G. Yodh acknowledges support from NIH 2-R01-HL57835-04.

References

- B. Chance, M. T. Dait, C. Zhang, T. Hamaoka, and F. Hagerman, "Recovery from exercise-induced desaturation in the quadriceps muscles of elite competitive rowers," *Am. J. Physiol.* **262**(3Pt 1), C766–775 (1992).
- T. Binzoni, L. Ngo, E. Hiltbrand, R. Springett, and D. Delpy, "Non-standard O(2) consumption-temperature curves during rest and isometric exercise in human skeletal muscle," *Comp. Biochem. Physiol., Part A: Mol. Integr. Physiol.* **132**(1), 27–32 (2002).
- D. J. Wallace, B. Michener, D. Choudhury, M. Levi, P. Fennelly, D. M. Hueber, and B. B. Barbieri, "Results of a 95-subject human clinical trial for the diagnosis of peripheral vascular disease using a near-infrared frequency domain hemoglobin spectrometer," *Proc. SPIE* **3597**, 300–316 (1999).
- T. R. Cheatele, L. A. Potter, M. Cope, D. T. Delpy, P. D. Coleridge Smith, and J. H. Scurr, "Near-infrared spectroscopy in peripheral vascular disease," *Br. J. Surg* **78**(4), 405–408 (1991).
- R. J. Whitney, "The measurement of volume changes in human limbs," *J. Physiol. (London)* **121**(1), 1–27 (1953).
- K. A. Engelke, J. R. Halliwill, D. N. Proctor, N. M. Dietz, and M. J. Joyner, "Contribution of nitric oxide and prostaglandins to reactive hyperemia in human forearm," *J. Appl. Physiol.* **81**(4), 1807–1814 (1996).
- J. R. Libonati, A. K. Howell, N. M. Incanno, K. K. Pettee, and H. L. Glassberg, "Brief muscle hypoperfusion/hyperemia: an ergogenic aid?," *J. Strength Cond. Res.* **15**(3), 362–366 (2001).
- J. R. Libonati, M. Cox, N. Incanno, S. K. Melville, F. C. Musante, H. L. Glassberg, and M. Guazzi, "Brief periods of occlusion and reperfusion increase skeletal muscle force output in humans," *Cardiologia* **43**(12), 1355–1360 (1998).
- R. Joannides, W. E. Haefeli, L. Linder, V. Richard, E. H. Bakkali, C. Thuillez, and T. F. Luscher, "Nitric oxide is responsible for flow-dependent dilatation of human peripheral conduit arteries in vivo," *Circulation* **91**(5), 1314–1319 (1995).
- C. Binggeli, L. E. Spieker, R. Corti, I. Sudano, V. Stojanovic, D. Hayoz, T. F. Luscher, and G. Noll, "Statins enhance postischemic hyperemia in the skin circulation of hypercholesterolemic patients: a monitoring test of endothelial dysfunction for clinical practice?," *J. Am. Coll. Cardiol.* **42**(1), 71–77 (2003).
- T. Binzoni, T. S. Leung, D. Boggett, and D. Delpy, "Non-invasive laser Doppler perfusion measurements of large tissue volumes and human skeletal muscle blood RMS velocity," *Phys. Med. Biol.* **48**(15), 2527–2549 (2003).
- R. S. Richardson, E. A. Noyszewski, L. J. Haseler, S. Bluml, and L. R. Frank, "Evolving techniques for the investigation of muscle bioenergetics and oxygenation," *Biochem. Soc. Trans.* **30**(2), 232–237 (2002).
- W. Burchert, S. Schellong, J. van den Hoff, G. J. Meyer, K. Alexander, and H. Hundeshagen, "Oxygen-15-water PET assessment of muscular blood flow in peripheral vascular disease," *J. Nucl. Med.* **38**(1), 93–98 (1997).
- V. Quaresima, M. Ferrari, M. A. Franceschini, M. L. Hoimes, and S. Fantini, "Spatial distribution of vastus lateralis blood flow and oxyhemoglobin saturation measured at the end of isometric quadriceps contraction by multichannel near-infrared spectroscopy," *J. Biomed. Opt.* **9**(2), 413–420 (2004).
- U. Wolf, M. Wolf, J. H. Choi, L. A. Paunescu, L. P. Safonova, A. Michalos, and E. Gratton, "Mapping of hemodynamics on the human calf with near infrared spectroscopy and the influence of the adipose tissue thickness," *Adv. Exp. Med. Biol.* **510**, 225–230 (2003).
- M. Ferrari, T. Binzoni, and V. Quaresima, "Oxidative metabolism in muscle," *Philos. Trans. R. Soc. London, Ser. B* **352**(1354), 677–683 (1997).
- R. A. De Blasi, M. Cope, C. Elwell, F. Safoue, and M. Ferrari, "Non-invasive measurement of human forearm oxygen consumption by near infrared spectroscopy," *Eur. J. Appl. Physiol.* **67**(1), 20–25 (1993).
- U. Wolf, M. Wolf, J. H. Choi, M. Levi, D. Choudhury, S. Hull, D. Coussirat, L. A. Paunescu, L. P. Safonova, A. Michalos, W. W. Mantulin, and E. Gratton, "Localized irregularities in hemoglobin flow and oxygenation in calf muscle in patients with peripheral vascular disease detected with near-infrared spectrophotometry," *J. Vasc. Surg.* **37**(5), 1017–1026 (2003).
- J. P. Culver, T. Durduran, D. Furuya, C. Cheung, J. H. Greenberg, and A. G. Yodh, "Diffuse optical tomography of cerebral blood flow, oxygenation, and metabolism in rat during focal ischemia," *J. Cereb. Blood Flow Metab.* **23**(8), 911–924 (2003).
- C. Cheung, J. P. Culver, K. Takahashi, J. H. Greenberg, and A. G. Yodh, "In vivo cerebrovascular measurement combining diffuse near-infrared absorption and correlation spectroscopies," *Phys. Med. Biol.* **46**(8), 2053–2065 (2001).
- G. Yu, T. Durduran, T. M. Busch, H. W. Wang, C. Zhou, H. M. Saunders, C. M. Seghal, and A. G. Yodh, "Non-Invasive Monitoring of hemodynamic responses in RIF tumors during and after PDT," *Proc. SPIE* **4952**, 131–139 (2003).
- D. A. Boas and A. G. Yodh, "Spatially varying dynamical properties

- of turbid media probed with diffusing temporal light correlation," *J. Opt. Soc. Am.* **14**(1), 192–215 (1997).
23. C. Menon, G. M. Polin, I. Prabhakaran, A. Hsi, C. Cheung, J. P. Culver, J. F. Pingpank, C. S. Sehgal, A. G. Yodh, D. G. Buerk, and D. L. Fraker, "An integrated approach to measuring tumor oxygen status using human melanoma xenografts as a model," *Cancer Res.* **63**(21), 7232–7240 (2003).
 24. T. Durduran, G. Yu, M. G. Burnett, J. A. Detre, J. H. Greenberg, J. Wang, C. Zhou, and A. G. Yodh, "Diffuse optical measurement of blood flow, blood oxygenation, and metabolism in a human brain during sensorimotor cortex activation," *Opt. Lett.* **29**(15), 1766–1768 (2004).
 25. E. R. Mohler, "Peripheral arterial disease: identification and implications," *Arch. Intern Med.* **163**(19), 2306–2314 (2003).
 26. R. B. Rutherford, J. D. Baker, C. Ernst, K. W. Johnston, J. M. Porter, S. Ahn, and D. N. Jones, "Recommended standards for reports dealing with lower extremity ischemia: revised version," *J. Vasc. Surg.* **26**(3), 517–538 (1997).
 27. L. A. Paunescu, "Tissue blood flow and oxygen consumption measured with near-infrared frequency-domain spectroscopy," PhD Thesis, University of Illinois, Urbana (2001).
 28. D. A. Boas, L. E. Campbell, and A. G. Yodh, "Scattering and Imaging with Diffusing Temporal Field Correlations," *Phys. Rev. Lett.* **75**(9), 1855–1858 (1995).
 29. D. J. Pine, D. A. Weitz, P. M. Chaikin, and E. Herbolzheimer, "Diffusing wave spectroscopy," *Phys. Rev. Lett.* **60**, 1134–1137 (1988).
 30. G. Maret and P. E. Wolf, "Multiple light scattering from disordered media. The effect of Brownian motion of scatterers," *Z. Phys.* **65**, 409–413 (1987).
 31. J. Mayhew, D. Johnston, J. Martindale, M. Jones, J. Berwick, and Y. Zheng, "Increased oxygen consumption following activation of brain: Theoretical footnotes using spectroscopic data from barrel cortex," *Neuroimage* **13**(6), 975–987 (2001).
 32. M. Ciccoira, L. Zanolla, L. Franceschini, A. Rossi, G. Golia, M. Zamboni, P. Tosoni, and P. Zardini, "Skeletal muscle mass independently predicts peak oxygen consumption and ventilatory response during exercise in noncachectic patients with chronic heart failure," *J. Am. Coll. Cardiol.* **37**(8), 2080–2085 (2001).
 33. S. Homma, H. Eda, S. Ogasawara, and A. Kagaya, "Near-infrared estimation of O₂ supply and consumption in forearm muscles working at varying intensity," *J. Appl. Physiol.* **80**(4), 1279–1284 (1996).
 34. V. Quaresima, S. Homma, K. Azuma, S. Shimizu, F. Chiarotti, M. Ferrari, and A. Kagaya, "Calf and shin muscle oxygenation patterns and femoral artery blood flow during dynamic plantar flexion exercise in humans," *Eur. J. Appl. Physiol.* **84**(5), 387–394 (2001).
 35. T. Binzoni, V. Quaresima, G. Barattelli, E. Hiltbrand, L. Gurke, F. Terrier, P. Cerretelli, and M. Ferrari, "Energy metabolism and interstitial fluid displacement in human gastrocnemius during short ischemic cycles," *J. Appl. Physiol.* **85**(4), 1244–1251 (1998).
 36. A. Kienle and T. Glanzmann, "In vivo determination of the optical properties of muscle with time-resolved reflectance using a layered model," *Phys. Med. Biol.* **44**(11), 2689–2702 (1999).
 37. T. J. Farrell, M. S. Patterson, and M. Essenpreis, "Influence of layered tissue architecture on estimates of tissue optical properties obtained from spatially resolved diffuse reflectometry," *Appl. Opt.* **37**(10), 1958–1972 (1998).
 38. M. C. van Beekvelt, M. S. Borghuis, B. G. van Engelen, R. A. Wevers, and W. N. Colier, "Adipose tissue thickness affects in vivo quantitative near-IR spectroscopy in human skeletal muscle," *Clin. Sci.* **101**(1), 21–28 (2001).
 39. R. E. Klabunde, "Cardiovascular Physiology Concepts [Online]" (03/08/2005), <http://www.cvphysiology.com/>
 40. T. Tenland, E. G. Sælerud, G. E. Nilsson, and P. A. Oberg, "Spatial and temporal variations in human skin blood flow," *Int. J. Microcirc.: Clin. Exp.* **2**(2), 81–90 (1983).
 41. P. O. Astrand, K. Rodahl, H. Dahl, and S. Stromme, *Textbook of Work Physiology*, 4th ed., S. B. Michael, S. Myles, B. Kathleen, C. Derek, and L. D. Jennifer, Eds., pp. 146–148, Human Kinetics, Champaign, IL (2003).
 42. M. H. Laughlin, "Skeletal muscle blood flow capacity: role of muscle pump in exercise hyperemia," *Am. J. Physiol.* **253**(5Pt 2), H993–1004 (1987).
 43. M. C. Van Beekvelt, W. N. Colier, R. A. Wevers, and B. G. Van Engelen, "Performance of near-infrared spectroscopy in measuring local O₂ consumption and blood flow in skeletal muscle," *J. Appl. Physiol.* **90**(2), 511–519 (2001).
 44. R. A. De Blasi, M. Ferrari, A. Natali, G. Conti, A. Mega, and A. Gasparetto, "Noninvasive measurement of forearm blood flow and oxygen consumption by near-infrared spectroscopy," *J. Appl. Physiol.* **76**(3), 1388–1393 (1994).
 45. J. R. Kappa, H. D. Berkowitz, R. Seestedt, and B. Chance, "Evaluation of calf muscle oxygen content using near-infrared reflectance (NIR) spectroscopy in patients with peripheral vascular disease," in *Vascular Surgery 2000*, J. R. Cohen, Ed., pp. 10–16, R. G. Landes Co. (1992).
 46. R. S. Richardson, E. A. Noyszewski, B. Saltin, and J. Gonzalez-Alonso, "Effect of mild carboxy-hemoglobin on exercising skeletal muscle: intravascular and intracellular evidence," *Am. J. Physiol. Regul. Integr. Comp. Physiol.* **283**(5), R1131–1139 (2002).
 47. D. M. Mancini, L. Bolinger, H. Li, K. Kendrick, B. Chance, and J. R. Wilson, "Validation of near-infrared spectroscopy in humans," *J. Appl. Physiol.* **77**(6), 2740–2747 (1994).
 48. R. A. De Blasi, S. Fantini, M. A. Franceschini, M. Ferrari, and E. Gratton, "Cerebral and muscle oxygen saturation measurement by frequency-domain near-infrared spectrometer," *Med. Biol. Eng. Comput.* **33**(2), 228–230 (1995).
 49. T. Muellner, A. Nikolic, W. Schramm, and V. Vecsei, "New instrument that uses near-infrared spectroscopy for the monitoring of human muscle oxygenation," *J. Trauma* **46**(6), 1082–1084 (1999).
 50. S. Nioka, D. Moser, G. Lech, M. Evangelisti, T. Verde, B. Chance, and S. Kuno, "Muscle deoxygenation in aerobic and anaerobic exercise," *Adv. Exp. Med. Biol.* **454**, 63–70 (1998).
 51. H. Miura, K. McCully, L. Hong, S. Nioka, and B. Chance, "Regional difference of muscle oxygen saturation and blood volume during exercise determined by near infrared imaging device," *Jpn. J. Physiol.* **51**, 599–606 (2001).
 52. J. F. Toussaint, K. K. Kwong, F. O. M'Kparu, R. M. Weisskoff, P. J. LaRaia, H. L. Kantor, and F. M'Kparu, "Perfusion changes in human skeletal muscle during reactive hyperemia measured by echo-planar imaging," *Magn. Reson. Med.* **35**(1), 62–69 (1996).
 53. J. F. Toussaint, K. K. Kwong, F. M'Kparu, R. M. Weisskoff, P. J. LaRaia, and H. L. Kantor, "Interrelationship of oxidative metabolism and local perfusion demonstrated by NMR in human skeletal muscle," *J. Appl. Physiol.* **81**(5), 2221–2228 (1996).
 54. J. S. Raynaud, S. Duteil, J. T. Vaughan, F. Hennel, C. Wary, A. Leroy-Willig, and P. G. Carlier, "Determination of skeletal muscle perfusion using arterial spin labeling MRI: validation by comparison with venous occlusion plethysmography," *Magn. Reson. Med.* **46**(2), 305–311 (2001).